Polypyridyl ruthenium complexes as coating agent for the formation of gold and silver nanocomposites in different media. Preliminary luminescence and electrochemical studies†‡

Cédric R. Mayer,*[a] Eddy Dumas,[a] Fabien Miomandre,[b] Rachel Méallet-Renault,[b] Fabienne Warmont,[c] Jacky Vigneron,[a] Robert Pansu,[b] Arnaud Etcheberry[a] and Francis Sécheresse[a]

Received (in Montpellier, France) 2nd June 2006, Accepted 1st August 2006
First published as an Advance Article on the web 29th August 2006
DOI: 10.1039/b607889c

Three polypyridyl ruthenium complexes, [(phen)$_2$Ru(2,2′-*p*-phenylene-bis(imidazo[4,5-*f*][1,10]) phenanthroline)](X)$_2$ (**1** · X$_2$), [(phen)$_2$Ru((4-pyridine)oxazo[4,5-*f*][1,10]phenanthroline)](X)$_2$ (**2** · X$_2$) and [(phen)$_2$Ru((3-thiophene)imidazo[4,5-*f*][1,10]phenanthroline)](X)$_2$ (**3** · X$_2$), X$^-$ = PF_6^- or Cl^-, have been used to functionalize and stabilize gold and silver nanoparticles in aqueous and non aqueous (acetonitrile) media. Direct interaction between the metallic nanoparticles and the ruthenium complexes was ensured by bidentate chelating phenanthroline (**1**), monodentate pyridine (**2**) or monodentate thiophene (**3**) groups. The influence of several parameters was studied in order to control the size, shape and stability of the nanocomposites thus formed: the nature of the metallic nanoparticles, the nature of the coating ruthenium complex, the ratio $R = [M^{n+}]/[Ru^{2+}]$ (M = Ag or Au) and the solvent. The colloidal solutions have been characterized by UV-Vis spectroscopy, transmission electron microscopy (TEM) and X-ray photoelectron spectroscopy (XPS). Preliminary electrochemical and luminescence measurements have shown the influence of the metallic nanoparticle on the properties of the ruthenium complexes.

Introduction

A large variety of nanomaterials have been synthesized from carbon[1] to silica,[2] metal chalcogenides,[3] lanthanide oxides[4] or metallic nanoparticles (NPs).[5] Special attention was recently devoted to nanocomposites (NCs) for which the conception is mainly governed by the target application. For example, latex NPs functionalized by a ligand with high affinity towards copper ions and doped by a correctly chosen fluorophore can be used as a selective fluorescent nanosensor,[6] and metallic oxide NPs surrounded by an organosilicon shell can be used as a fluorescent biological probe.[7] Within the ever-growing field of nanosciences, NCs based on gold or silver nanoparticles have certainly attracted the most attention. Among them a large class of NPs coated by a stabilizer bearing terminal "active" groups such as DNA,[8] fullerene,[9] or ferrocenyl[10] has been described. The variety of functionalized silver or gold particles can be explained by their affinity with different donor ligands such as alkanethiols,[11] carboxylates,[12] phosphines[13] or amines.[14]

Our group was interested in the formation of nanocomposites by functionalization of gold or silver NPs with inorganic systems. The first inorganic entities used were pre-functionalized polyoxometalates,[15] and tetra(oxo)thiometalate.[16] Very recently, we employed another type of inorganic system as a coating and functionalizing agent, namely modified polypyridyl ruthenium complexes, in acetonitrile.[17] One of the three phenanthroline ligands chelating the ruthenium centre was modified to fix a terminal pyridine or phenanthroline group. The electron lone pair carried by the nitrogen atom(s) of the pyridine or phenanthroline terminal group ensured a strong interaction with the silver surface.[18] The originality of this work lies in the connection between the silver particles and the ruthenium complexes which is provided by fully π-conjugated systems.

Here we extended this original approach to gold nanoparticles in aqueous and non-aqueous (acetonitrile) medium using three ruthenium complexes, [(phen)$_2$Ru(2,2′-*p*-phenylene-bis (imidazo[4,5-*f*][1,10])phenanthroline)](X)$_2$ (noted **1** · X$_2$), [(phen)$_2$Ru((4-pyridine)oxazo[4,5-*f*][1,10]phenanthroline)](X)$_2$ (noted **2** · X$_2$) and [(phen)$_2$Ru((3-thiophene)imidazo[4,5-*f*'][1,10]phenanthroline)](X)$_2$ (noted **3** · X$_2$), X$^-$ = PF_6^- or Cl^-.

[a] *Institut Lavoisier de Versailles, UMR 8180, Université de Versailles, 45 Avenue des Etats-Unis, 78035 Versailles, France. E-mail: cmayer@chimie.uvsq.fr; Fax: +33 1 39 25 43 81; Tel: +33 1 39 25 43 97*
[b] *Laboratoire PPSM, UMR 8531, Ecole Normale Supérieure de Cachan, 61 Avenue du Président Wilson, 94235 Cachan, France*
[c] *Laboratoire de Réactivité de Surface, UMR 7609, Université Paris 6, 4 Place Jussieu, 75252 Paris Cedex 05, France*

† The HTML version of this article has been enhanced with colour images.

‡ Electronic Supplementary Information (ESI) available: ESI-MS spectra of L-thiophene (Fig. S1) and **3** · Cl$_2$ (Fig. S2); MALDI-TOF spectrum of **3** · Cl$_2$ (Fig. S3); TEM image of Au-**3**-NCs synthesized in acetonitrile (Fig. S4); TEM image of Au-**2**-NCs after flocculation in acetonitrile and re-dispersion in water, and corresponding absorption spectrum in water (Fig. S5); XPS spectra of Au 4f and Cl 2p regions (Fig. S6); TEM images of Au-**2**-NCs (Fig. S7) and Ag-**3**-NCs (Fig. S8) in water; cyclic voltammograms of Au-**1**-NCs and Au-**3**-NCs in acetonitrile (Fig. S9). See DOI: 10.1039/b607889c.

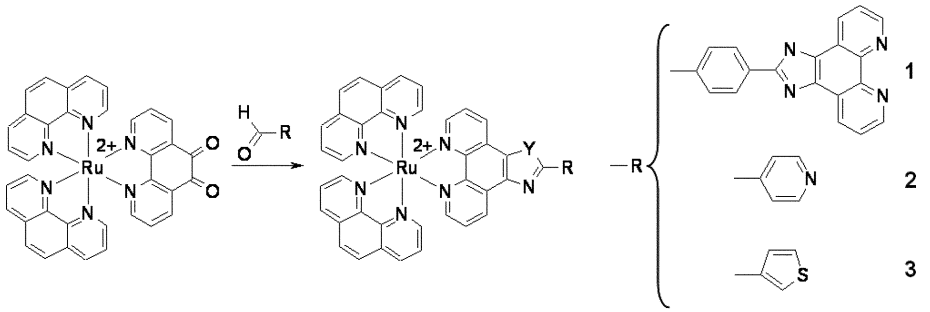

Scheme 1 Structure of the three ruthenium complexes used to stabilize and functionalize the metallic nanoparticles. Y = NH for **1** and **3** and Y = O for **2**.

The three complexes are synthesized by reaction of $[(phen)_2Ru(phen\text{-}dione)]Cl_2$ with the appropriate aldehyde (Scheme 1). The aim of this work is to study the interaction of the various terminal groups (bidentate chelating phenanthroline (**1**), monodentate pyridine (**2**) and monodentate thiophene (**3**)) with the metallic surface. Indeed, any future potential application would necessarily require an effective control of the size, shape and monodispersity of these NCs considering that these are key factors for electronic and optical properties. Preliminary electrochemical and luminescence measurements were also undertaken to show the influence of the metallic nanoparticle on the electrochemical and luminescence properties of the ruthenium complex.

Experimental

General

All reagents and solvents were purchased from Acros, Aldrich, Avocado or SDS and used as received. All aqueous solutions were prepared using ultrapure water purified with a Millipore-Q$^+$ system. $[(phen)_2Ru(2,2'\text{-}p\text{-}phenylene\text{-}bis(imidazo[4,5\text{-}f][1,10])phenanthroline)](PF_6)_2$ (**1**),[17] $[(phen)_2Ru((4\text{-}pyridine)oxazo[4,5\text{-}f][1,10]phenanthroline)](PF_6)_2$ (**2**),[17] $(phen)_2RuCl_2$,[19] 1,10-phenanthroline-5,6-dione (noted phendione),[20] and $[(phen)_2Ru(phendione)]Cl_2$,[20] were synthesized following the procedure previously reported.

Visualization of gold nanoparticles was performed with a transmission electron microscope (microscope JEOL 2010 UHR) in the "Centre Régional de Mesures Physiques" Paris 6: a drop of diluted solution was deposited and dried on a grid.

X-Ray photoelectron spectroscopy (XPS) measurements were performed on a VG ESCALAB 220i-XL system using monochromatized Al $K\alpha_1$ excitation. High resolution spectra were recorded using a constant analysis energy mode in high resolution configuration (pass energy of 20 or 8 eV). The photoelectrons were collected perpendicularly to the surface holder (Si plane wafer). Curve fitting was performed using the Eclipse data system developed by VG Scientific. The spectrometer calibration was carried out on Cu, Ag and Au samples following the ASTME 902-94 standard procedure. The Au $4f_{7/2}$ peak on an etched Au foil had a binding energy of 84.0 eV.

UV/Vis spectra were recorded using a Perkin Elmer UV/Vis/NIR lambda 19 PC scanning spectrophotometer. Each sample was analyzed in a similar way: 0.1 mL of colloidal solution was diluted in 2.9 mL of similar solvent. ^1H (300 MHz) NMR spectra were obtained at room temperature in 5 mm o.d. tubes on a Bruker Avance 300 spectrometer equipped with a QNP probe head.

ESI-MS measurements were carried out with a HP 5989B single quadrupole mass spectrometer equipped with an electrospray source from Analytica of Branford. The instrument was operated in the positive ion mode. The MALDI-TOF mass spectra were recorded using a Voyager Elite time-of-flight mass spectrometer (PerSeptive Biosystems, Boston, MA, USA). All MALDI-TOF mass spectra were recorded and averaged over 256 laser shots by a Tektronix TDS 520 oscilloscope (Beaverton, OR, USA).

Syntheses

Synthesis of 3-thiophenimidazo[4,5-*f*][1,10]phenanthroline (denoted L-thiophene). A mixture of 3-thiophenecarboxaldehyde (105 μL, 1.2 mmol), NH_4OAc (1.54 g, 20 mmol) and phendione (0.21 g, 1 mmol) in acetic acid (30 mL) was stirred at reflux for 4 h. The mixture was then cooled at room temperature and the pure crude product precipitated during the neutralization of the mixture with concentrated aqueous ammonia. The precipitate was filtrated, washed with water and dried with diethyl ether to give the pure product. L-thiophene. Yield: 0.23 g, 76%. δ_H (300 MHz; DMSO-d*6*) 13.5 (s, 1H; NH), 9.0 (dd, J = 4.2, 1.5 Hz, 2H; phenH), 8.88 (dd, J = 8.1, 1.5 Hz, 2H; phenH), 8.33 (dd, J = 2.7, 1.2 Hz, 1H; thiopH), 7.90 (d, J = 5 Hz, 1H; thiopH), 7.78–7.82 (dd, J = 8.1, 4.5 Hz, 2H; phenH), 7.75 (dd, J = 5.1, 3 Hz, 1H; thiopH); ESI-MS (Fig. S1‡), m/z 303.2 (MH^+), $[C_{17}H_{10}N_4S]^{2+}$ theoretical m/z 303.3 (monoisotopic ion).

Synthesis of $[(phen)_2Ru(3\text{-}thiophenimidazo[4,5\text{-}f][1,10]phenanthroline)](PF_6)_2$ ($\mathbf{3}\cdot(PF_6)_2$)

Method A. A mixed solution (EtOH–H_2O–DMF: 40 : 10 : 5 mL) of $(phen)_2RuCl_2$ (100 mg, 0.19 mmol) and L-thiophene (60 mg, 0.20 mmol) was refluxed overnight. The mixture was cooled at room temperature, 40 mL of deionized water was added and the crude product was precipitated by addition of a concentrated aqueous solution of NH_4PF_6. The precipitate was filtrated, washed and dried with diethyl ether. Crystallization of the crude product by slow diffusion of diethyl ether in acetonitrile gives an orange pure product. Yield 168 mg, 84% (Found: C, 47.16; H, 2.69; N, 11.21; Ru, 9.26; S, 2.93. $C_{41}H_{26}F_{12}N_8SP_2Ru$ requires C, 46.73; H, 2.5; N, 10.63; Ru,

9.59; S, 3.04%). ESI-MS (Fig. S2‡): m/z 382.3, $[C_{41}H_{26}N_8SRu]^{2+}$ theoretical m/z 381.9 (monoisotopic ion). MALDI-TOF, positive ion mode (Fig. S3‡): m/z 764.1, theoretical m/z 763.9.

Method B. A solution of $[(phen)_2Ru(phendione)]Cl_2$ (100 mg, 0.135 mmol), NH_4OAc (210 mg, 2.7 mmol) and 3-thiophenecarboxaldehyde (17 μL, 0.195 mmol) in acetic acid (17.4 M, 25 mL) was stirred at 120 °C for 6 h and then cooled to room temperature. The solution was neutralized with concentrated aqueous ammonia and 200 mL of deionized water was added. The product was precipitated by addition of a concentrated aqueous solution of NH_4PF_6, filtrated, washed with water and dried with diethyl ether. The pure product was re-precipitated from an acetonitrile solution by the addition of diethyl ether. Yield 111 mg, 78%.

Synthesis of $1\cdot Cl_2$, $2\cdot Cl_2$ and $3\cdot Cl_2$. Chloride salts of **1**, **2** and **3** were precipitated from acetone solutions of the corresponding hexafluorophosphate salts by addition of tetrabutylammonium chloride.

Preparation of Au- and Ag-NPs coated with 1, 2 or 3. All syntheses were carried out with 29.5 μmol of silver(I) nitrate (5 mg) or chloroauric acid trihydrate (11.6 mg) in 20 mL of solvent (acetonitrile or deionized water). The molar concentration ratio $R = [M^{n+}]/[Ru^{2+}]$ (M = Ag or Au) and the volume of reducing agent added (aqueous solution of $NaBH_4$ with a molar concentration of 0.4 M, systematically added at once) were the adjustable parameters. Hexafluorophosphate salts of the ruthenium complexes were used in acetonitrile and chloride salts were used in water.

Preparation of Au-1-NCs, Au-2-NCs and Au-3-NCs in water. $HAuCl_4\cdot 3H_2O$ (11.6 mg, 29.5 μmol) was dissolved in 20 mL of water and $\mathbf{1}\cdot Cl_2$ (15.7 mg, 15 μmol, $R = 2$), $\mathbf{2}\cdot Cl_2$ (12.5 mg, 15 μmol, $R = 2$) or $\mathbf{3}\cdot Cl_2$ (24.6 mg, 29.5 μmol, $R = 1$) was added. An aqueous solution of $NaBH_4$ (120 μL, 0.4 M) was then added. Depending on the R ratio and the nature of the ruthenium complex, a more or less abundant precipitate formed after reduction of Au(III).

Preparation of Ag-1-NCs, Ag-2-NCs and Ag-3-NCs in water. The NCs were prepared according to the above described procedure using $AgNO_3$ (5 mg, 29.5 μmol) instead of $HAuCl_4\cdot 3H_2O$ and 120 μL of $NaBH_4$ (0.4 M) in all cases.

Preparation of Au-1-NCs, Au-2-NCs, Au-3-NCs, and Ag-3-NCs in acetonitrile. The above procedure was used, employing the hexafluorophosphate salts of **1**, **2** and **3** instead of the corresponding chloride salts. 240 μL of $NaBH_4$ (0.4 M) were used, which implies a small excess of reducing agent, except when specifically stated in the text.

Electrochemical measurements

Electrochemical measurements were performed in a three electrode cell equipped with a 1 mm diameter platinum disk as the working electrode, platinum wire as the counter electrode and Ag^+(0.01 M)/Ag as the reference electrode. The reference potential was checked *vs*. ferrocene as recommended by IUPAC ($E^\circ = +92$ mV). The supporting electrolyte was hexafluorophosphate tetrabutylammonium (Fluka, puriss.) and the solutions were deaerated by argon bubbling prior each experiment. Cyclic voltammograms (CVs) were recorded with a home made potentiostat equipped with a tuneable ohmic drop compensation system.[21]

Luminescence measurements

UV-visible absorption spectra were measured with a Varian CARY 500 spectrophotometer from 280 to 800 nm. Emission spectra were measured on a SPEX Fluorolog-3 (Jobin-Yvon), with a 453 nm excitation wavelength. All solvents were of spectroscopic grade. Optical density was adjusted below 0.1 to avoid reabsorption artefacts. The solutions were deaerated by argon bubbling prior to each experiment. DCM (4-(dicyanomethylene)-2-methyl-6-(*p*-dimethylaminostyryl)-4*H*-pyran) in methanol was used as a reference to measure luminescence quantum yields.[22]

Results and discussion

Synthesis and characterization

Au-nanocomposites (Au-NCs) in acetonitrile

Characterization by TEM and UV-Vis spectroscopy. A preliminary comment must be made about the molar ratio of reducing agent ($NaBH_4$) used. The formation of Au-**1**-NCs, varying the amount of $NaBH_4$, was followed by UV-Vis spectroscopy (Fig. 1). Addition of 120 μL of $NaBH_4$ (0.4 M), sufficient to completely reduce an equivalent amount of silver(I) nitrate,[17] did not allow the complete reduction of $HAuCl_4$. If 120 μL of $NaBH_4$ (0.4 M) are used to reduce Au(III), the UV-Vis spectrum of Au-**1** ($R = 6$) displays the expected surface plasmon band (SPB) at 530 nm, the MLCT band of **1** at 453 nm but also an additional band at 322 nm assigned to gold-to-ligand charge transfer.[23] This band is present for all $R = [Au^{3+}]/[\mathbf{1}]$ ratios confirming that under these conditions Au(III) is only partially reduced. However, a twofold increase in the quantity of $NaBH_4$ (240 μL of $NaBH_4$ (0.4 M) leading to a small excess of reducing agent) led to the complete reduction of Au(III) confirmed by the disappearance of the band at 322 nm and the presence of a strong SPB at 543 nm, separated from the MLCT band of **1** at 453 nm.

In acetonitrile, for all R ratios and for the three ruthenium complexes, only nearly spherical NCs were obtained (Fig. 2). Au-**1**-NCs and Au-**2**-NCs showed similar behavior, namely an increase in the size of the NCs together with an increase in the polydispersity when the ratio R is increased. Typical size values are reported in Table 1.

A specific behavior was observed with Au-**3**. An immediate flocculation occurred when 240 μL of $NaBH_4$ (0.4 M) were used to reduce Au(III) in the presence of **3**. Stable colloidal solutions were characterized when using 80 μL of $NaBH_4$ (0.4 M), with a good monodispersity and a correlation between the ratio $R = [Au^{3+}]/[Ru^{2+}]$ and the size of the NCs. With $R = 2$, TEM analysis revealed a large majority of Au-**3**-NCs with a size of 2 ± 1 nm together with a very small amount of larger particles up to 10 nm (Fig. S4 of the ESI‡), while with $R = 6$, larger NCs were observed (8 ± 2 nm) and only a very small amount of smaller particles were identified. This general

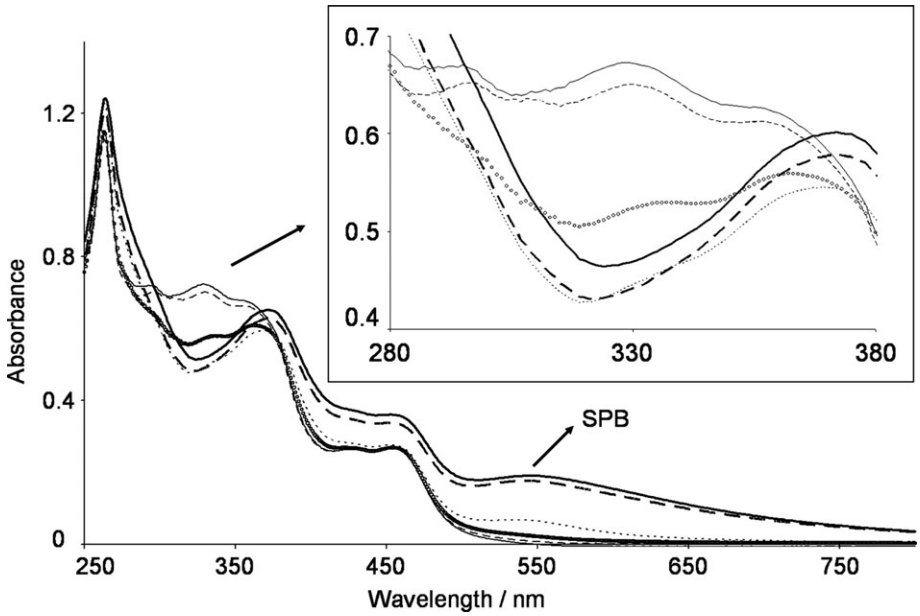

Fig. 1 Absorption spectra of Au-**1** in acetonitrile (R = 6) using different amounts of $NaBH_4$ and expansion of the N-to-gold charge transfer region. 0 μL (full line), 80 μL (dashed line), 120 μL (empty circles), 160 μL (dotted line), 200 μL (bold dashed line) and 240 μL (bold full line) of $NaBH_4$ (0.4 M).

behavior can be explained by a weak interaction between Au-NPs and **3**. Stable colloidal solutions were obtained only when a large excess of **3** was introduced to stabilize the Au-NCs.

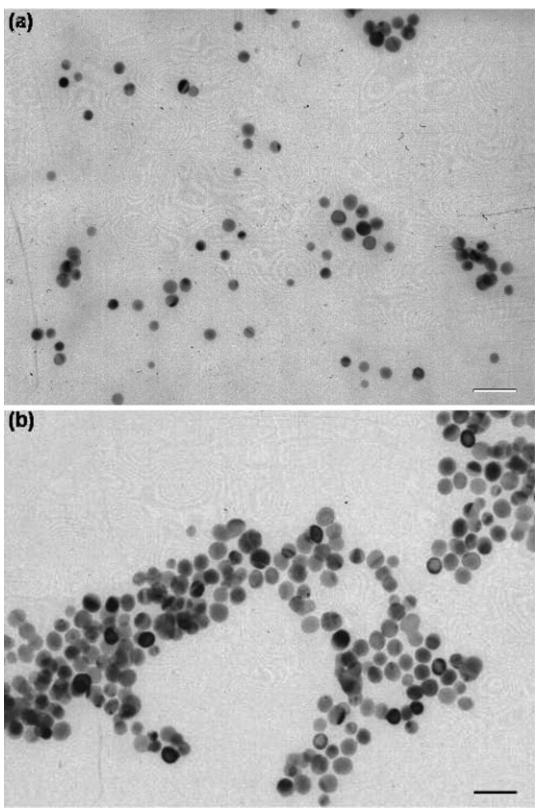

Fig. 2 TEM images of (a) Au-**1** (R = 2) and (b) Au-**2** (R = 2), in acetonitrile. Scale: 30 nm.

In addition to the effect on the size of the Au-NCs (see above), the ratio $R = [Au^{3+}]/[\mathbf{1}]$ drastically influences the stability of the colloidal solutions. For R = 2, the solutions are stable for months while for R = 6 and 10 flocculation is observed after only few hours. After the flocculate was centrifuged and re-dispersed in aqueous solution, the resulting hydrosols of Au-**1** remained stable for months. TEM examination of the hydrosols revealed slightly larger particles than in acetonitrile solutions, and the presence of few polygonal particles (Fig. S5a‡). UV-Vis spectra of the aqueous colloidal solutions also showed a SPB at 540 nm (Fig. S5b‡). The

Table 1 Summary of the characteristics of the different NCs isolated in water and acetonitrile

	CH_3CN			H_2O		
NCs	R^a	Shape	Size/nm	R^a	Shape	Size/nm
Au-**1**	2	Spherical	6 ± 2	2	Facetted	16–25[h]
	6	Spherical[b]	16 ± 2			
	10	Spherical[b]	22 ± 8			
Au-**2**	2	Spherical	10 ± 2	2	Facetted	15–30
	6	Spherical[b]	12–20[c]			
Au-**3**	2[d]	Spherical	2 ± 1[e]	1	Facetted	10–25
	6[d]	Spherical	8 ± 2[f]			
Ag-**1**	2[g]	Spherical	2 ± 1	2, 6	Spherical	25–35[f]
	10[g]	Spherical	8–10	10		
Ag-**2**	2[g]	Spherical	8 ± 1	2	Spherical	8 ± 2[h]
	10[g]	Spherical	10–20	6, 10	Spherical	5–15
Ag-**3**	2[b]	Spherical	10 ± 3[h]	1, 2	Spherical	5–10[h]
	6[b]	Spherical	10–40	3, 6		

[a] $R = [M^{n+}]/[Ru^{2+}]$ with $M^{n+} = Au^{3+}$ or Ag^+. [b] Aggregation in acetonitrile and stable after re-dispersion in water. [c] Presence of a small amount of larger particles up to 50 nm. [d] 80 μL of $NaBH_4$ (0.4 M). [e] Presence of a small amount of larger particles up to 10 nm. [f] Presence of a small amount of smaller particles. [g] See ref. 17. [h] Presence of a small amount of larger particles.

behavior of Au-**1**-NCs in acetonitrile for $R = 6$ and 10 can be interpreted considering that a large amount of chloride anions was released by the Au(III) precursor, $HAuCl_4$, leading to high $[Cl^-]/[\mathbf{1}]$ ratios ($[Cl^-]/[\mathbf{1}] = 24$ and 40 for $R = 6$ and 10, respectively). It is therefore possible to expect an anionic exchange between the hexafluorophosphate and the chloride anions in the vicinity around the Au-**1**-NCs generating flocculation in acetonitrile.[24] The flocculate of NCs, mainly surrounded by chloride anions, can subsequently be easily re-dispersed in water. This hypothesis of a spontaneous anionic exchange, leading to a purification of the nanocomposites, was confirmed by XPS analysis.

*Characterization by XPS of Au-**1**-NCs ($R = 6$) synthesized in acetonitrile and re-dispersed in water*. For XPS characterizations, slabs of deoxidized Si were coated with drops of Au-NCs particles dispersed in ultra pure water and dried under a N_2 stream. The XPS spectra are consequently specific to the lone Au-NCs structure in contact with the Si support. The analyses were performed on several drops. The data are reproducible for the determined chemical composition as well as for the energy distribution of the peak obtained for the Au_{4f}, Cl_{2p}, Ru_{3d}-C_{1s}, O_{1s} and N_{1s} regions that we have explored. It confirmed the purification process induced by the anionic exchange. Moreover, duration tests under X-ray lightning have been performed without evidence of sample degradation. Therefore the system must be considered as stable and the results can be interpreted as the direct X-photoelectron fingerprint of the functionalized particles. Table 2 summarizes the characteristic ratios obtained between the N, C, Cl, Ru and Au elements. These values are obtained using the peak area of the core level peak of each element corrected by their respective sensitivity factors. Fig. 3 shows the C_{1s}, Ru_{3d} and N_{1s} regions with in each case multicomponent fitting which shows clearly the feature characteristics of the different chemical sites (see Fig. S6 of the ESI for Au_{4f} and Cl_{2p} regions‡). The spectra presented in Fig. 3 are the experimental spectra without any global correction.

Several key features can be extracted from the XPS analysis of Au-**1**-NCs ($R = 6$). The first result concerns the Ru/Au ratio of ~5.2. The Au-NPs have a mean diameter of 16 nm, so we can consider that the amount of Au is important and therefore the ratio can be interpreted as resulting from the capping and the buried position of the particle. Considering the proposed orientation of the ruthenium complexes at the surface of the Au-NPs (Scheme 2), it is evident that the final Ru/Au ratio has to reflect the fact that the Au photoelectrons must escape through a probably dense structure, which implies a loss of signal, while those associated to Ru come from outer sites. Therefore the ratio cannot be used directly to measure the value of the exact coverage of Ru complexes normalized by the Au atom surface density. However, the very reproducible value demonstrates a very regular coating phenomenon. More precise coverage estimation would imply working on a flat Au surface in order to provide a quantitative interpretation of the Ru/Au ratio.

Table 2 Ratios between elements determined by XPS for $\mathbf{1} \cdot Cl_2$, Au-**1**-NCs ($R = 6$) precipitated in acetonitrile and re-dispersed in water. Theoretical ratios are given in brackets

	N/Ru	C/Ru	Cl/Ru	Ru/Au
$\mathbf{1} \cdot Cl_2$	13.2 (12)	71.9 (56)	1.9 (2)	—
Au-**1**-NCs	16.6 (12)	74.3 (56)	0.8	5.2

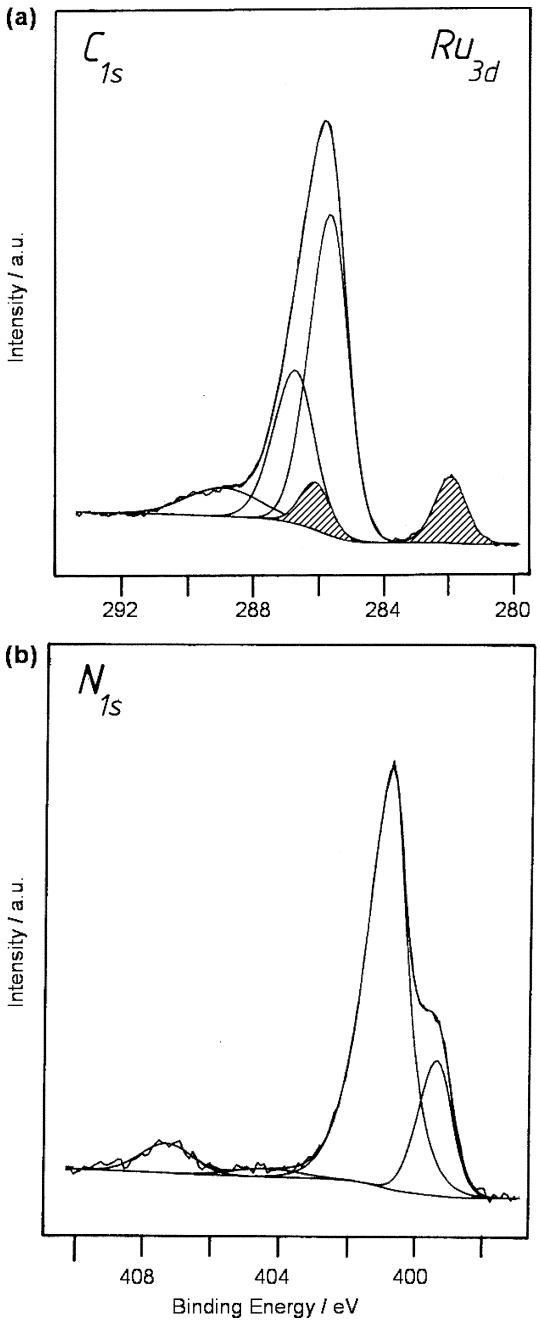

Fig. 3 Experimental XPS spectra of (a) C 1s and Ru 3d (hatched peaks) and (b) N 1s of Au-**1**-NCs. See Table 3 for the binding energy of the deconvoluted peaks.

Concerning the gold particles, the Au $4f_{7/2}$ signal is detected around 84.9 ± 0.2 eV for different drops. This position differs slightly from that of 84 eV observed for bulk Au systems. The shape of the peak is compatible with the pure metallic character of the signal and the shift of ~0.9 eV can be attributed to the interaction of the Au-NCs with the Si wafer used as the

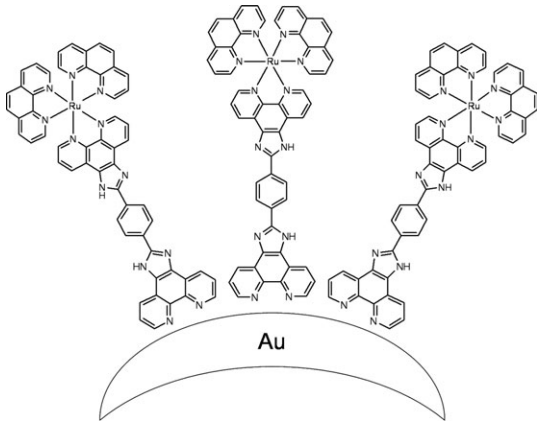

Scheme 2 Schematic view of the proposed orientation of the ruthenium complexes at the surface of the Au-NCs.

surface holder. The raw data together with the data corrected from the 0.9 eV shift are summarized in Table 3. The corrected values will be used in the following discussion.

The presence of a Cl 2p signal at 197.3 eV, attributable to ionic Cl^-,[25] confirmed the hypothesis of an anionic exchange between the hexafluorophosphate and chloride ions in the close shell around the Au-**1**-NCs leading to the precipitation in acetonitrile and to the possible re-dispersion in water of the flocculate thus generated. The rather reproducible Cl/Ru ratio suggests that the chloride anions play their role of counterion perfectly in a very stable structure.[26]

The highly reproducible energy distance (3.8 eV) between the Ru $3d_{5/2}$ and the C 1s positions must be emphasized and can be considered as the result of a well-preserved structure of the ruthenium complex at the Au NP surface (Fig. 3a). This distance also confirmed the +II oxidation state of the ruthenium in the complex.[27] The integrity of the structure of the ruthenium complex can also be corroborated by the ratios N_{1s}/Ru_{3d} and C_{1s}/Ru_{3d}. If the slightly higher value observed for the ratio C_{1s}/Ru_{3d} can be interpreted by a tedious carbon contamination, the constant and reproducible ratio N_{1s}/Ru_{3d}, that can be considered as the best internal probe of the polypyridyl ligands/Ru ratio, is totally specific to the Ru complex structure.

Finally, an important feature of the XPS analysis concerns the N 1s signals. The N 1s signals are deconvoluted in three major peaks located at 398.6 (noted A), 400.2 (B) and 406.5 (D) eV while a fourth and less intense peak is observed at 403.5 (C) eV. N 1s signal at *ca.* 408 eV is generally attributed to nitrate anions.[28] However, the presence of such an amount of nitrate anions in our sample can be ruled out. It has to be noted that the ratios involving the different peaks are remarkably constant over several drops of Au-**1**-NCs (Table 3). The peak centered at 400.2 eV (B) can be tentatively assigned to the six nitrogen atoms surrounding the ruthenium center.[29] The six remaining nitrogen centers, 4 nitrogen atoms of the two imidazole functions and 2 nitrogen atoms of the terminal phenanthroline group, can therefore be tentatively separated in two groups and observed at 398.6 (A) and 406.5 (D) eV, respectively. The difference between the experimental ratios of the peak area percentages (B/A = 4.1, D/A = 0.33) and the theoretical atomic percentage ratios (B/A = 1.5, D/A = 0.5) can be explained by an orientation of the ruthenium complexes at the gold surface as shown in Scheme 2. Intensity of the outer nitrogen atoms (B) will be exalted compared with the inner nitrogen atoms (A and D). Such an assignment would indeed imply a strong effect of the Au-NP on the binding energy of the nitrogen atoms of the phenanthroline pendant group directly connected to the particle. XPS measurements, using Au-NP coated by various ruthenium complexes, are currently under way in order to unambiguously assign the peaks to the different nitrogen atoms and also in order to better understand the effect of the Au-NP on the binding energy of the nitrogen atoms directly connected to the gold surface.

Ag-nanocomposites (Ag-NCs) in acetonitrile. Stabilization of Ag-NPs by **1** and **2** has already been described.[17] Complexes **1** and **2** ensured an effective coating of silver particles, even with a low amount of complexes. For both complexes, the control of the size of the nearly spherical Ag-NCs was obtained by varying the ratio $[Ag^+]/[Ru^{2+}]$. The resulting colloidal solutions were stable during several weeks and no modification of Ag-NCs was detected by TEM or UV-Vis spectroscopy.

As already observed in the case of Au-NPs coated by **3**, a weak interaction between Ag-NPs and **3** was also observed leading to nearly spherical and polydisperse NCs. The Ag-NCs colloidal solutions thus obtained were stable for one week with $R = 2$ while a precipitation was observed after only few seconds with $R = 6$. Both solids were easily re-dispersed in water after subsequent treatment of the initial acetonitrile solution. This behavior can be explained by a spontaneous exchange of the surrounding anions PF_6^- by NO_3^- (brought by $AgNO_3$) leading to precipitation in acetonitrile but allowing re-dispersion in water. This anionic exchange is similar to that described above between PF_6^- and Cl^- for Au-NCs in acetonitrile.

Au-nanocomposites (Au-NCs) in water. . For ratios $R > 2$ aggregation occurred. For the ruthenium complexes **1** and **2**, stable colloidal solutions were obtained only when a large amount of Ru(II) complex was used (typically up to $R = 2$). For ratios $R > 2$ aggregation occurred. In the case of Au-**3**-NCs, the weak interaction of the thiophene pendant group

Table 3 Binding energy (BE/eV) and relative peak area (%) of the Au 4f, Cl 2p, Ru 3d, C 1s and N 1s regions. Raw data and corrected values with respect to the Au $4f_{7/2}$ fixed at 84.0 eV

	Au $4f_{7/2}$	Cl 2p	Ru $3d_{5/2}$	Ru $3d_{3/2}$	C 1s	C 1s	C 1s	N 1s (A)	N 1s (B)	N 1s (C)	N1s (D)
Raw BE/eV	84.9	198.2	282.0	286.2	285.9	286.9	289.0	399.5	401.1	404.4	407.4
Corrected BE/eV	84.0	197.3	281.1	285.3	285.0	286.0	288.1	398.6	400.2	403.5	406.5
Peak area (%)	100	100	100	100	60	30	10	18	74	2	6

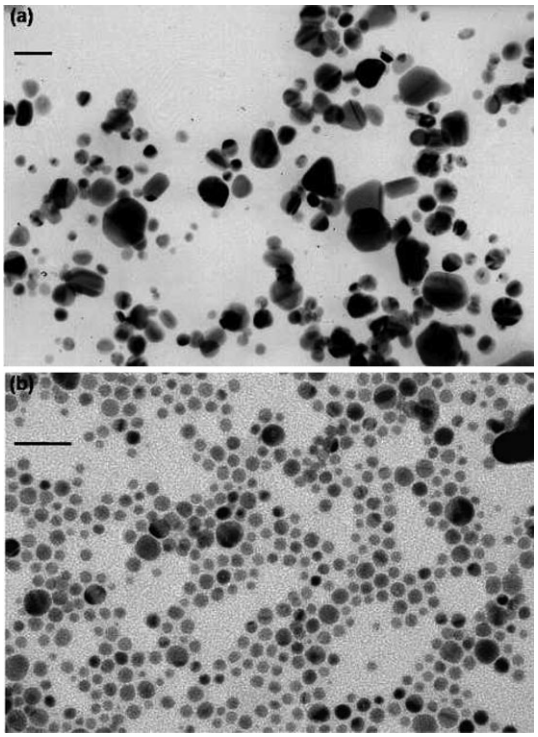

Fig. 4 TEM images of (a) Au-**2**-NCs and (b) Ag-**2**-NCs, in water (R = 2) showing the influence of the nature of the metallic particle for the final shape of the NCs. Scale: 30 nm.

with the gold surface was again observed. A stable colloidal solution of facetted and polydisperse particles was only obtained with the ratio R = 1 (Fig. S7‡). For all ruthenium complexes, TEM analysis revealed the presence of several facetted particles with triangular, pentagonal or hexagonal shapes (Fig. 4a).

Ag-nanocomposites (Ag-NCs) in water. Stable colloidal solutions were obtained for all R ratios studied with the three ruthenium complexes. Only near-spherical NCs were observed with Ag in water with the three ruthenium complexes studied (Fig. 4b). The nature of the metallic particles is therefore a key factor to determine the final shape of the NCs in water.

TEM and UV-Vis analyses showed that, contrary to what was observed with Au-NCs in water, no noticeable influence of R was observed on the final size or shape of the silver NCs. In the case of Ag-**1**-NCs, particles with a mean diameter of 30 nm were obtained with a slight increase in the polydispersity when R increases. A similar concomitant increase in the polydispersity with R was detected with Ag-**2**-NCs. A majority of Ag-**3**-NCs of 5–10 nm were observed together with a minority of larger particles, up to 20 nm (Fig. S8‡).

Preliminary electrochemical and luminescence properties

The electrochemical and luminescence properties have been studied with Au-NCs synthesized in acetonitrile since these systems afforded the most monodisperse colloidal solutions (Fig. 2).

Electrochemistry of Au-NCs in acetonitrile. Au-**1**-NCs and Au-**3**-NCs in acetonitrile exhibit, an irreversible and a partially reversible oxidation wave for the Ru(II)/Ru(III) redox couple, respectively (see the ESI for corresponding CVs, Fig. S9‡). This lack of reversibility, which was also observed for the corresponding free ruthenium complexes, could be due to chemical coupling of the oxidized form of **1** and **3** through the terminal phenanthroline or thiophene ligands, respectively. This means that for these two compounds oxidation may involve not only the metal centre but also the terminal ligand through cation radical formation.

The CV of Au-**2**-NCs in acetonitrile shows a single and fully reversible oxidation wave corresponding to the Ru(II)/Ru(III) redox couple (Fig. 5) and this was thus selected for further investigation. From the single character of the wave we can conclude that all the ruthenium moieties are oxidized at the same potential, like in many other multiple redox moiety functionalized systems.[30] Such behavior is generally observed either with non-interacting redox moieties, or with fully conjugated systems where a large number of oxidation (or reduction) states very close in energy are accessible (like in conducting polymers). In the first case, we should normally observe a single wave with a peak current corresponding to a number of electrons exchanged equal to the total number of redox sites on the particle, but with a peak-to-peak separation corresponding to one exchanged electron,[31] while in the second case multiple charge injection usually results in somewhat broader voltammetric waves.

In order to discuss the influence of the NP on the electrochemical response of the ruthenium complex, we focused on the comparison between the grafted ruthenium complex in Au-**2**-NCs and the free ruthenium complex **2** (Fig. 6 and Table 4). Both CVs correspond to the same concentration in ruthenium and to the same experimental conditions. We can see clearly that the standard potential associated to the grafted ruthenium complex is slightly lower than that of the free complex, while the peak-to-peak separation remains fairly constant. These results tend to show that the ruthenium centres are not electrostatically interacting, since the gold nanoparticle slightly stabilizes the more charged state of the complex,

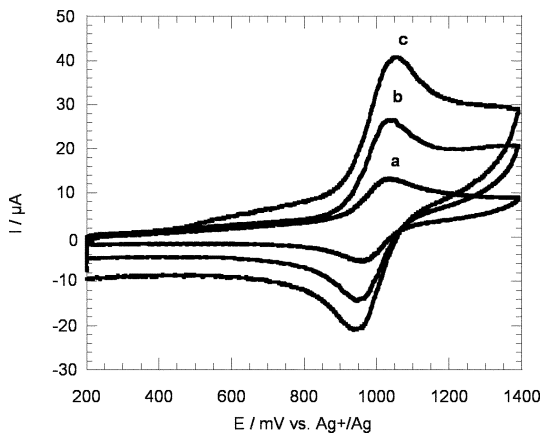

Fig. 5 CVs of Au-**2**-NCs in acetonitrile (R = 2; TEM image, see Fig. 2b) on a platinum electrode at various scan rates: a) 1; b) 5; c) 10 V s^{-1}. Concentration of ruthenium: 1 mM.

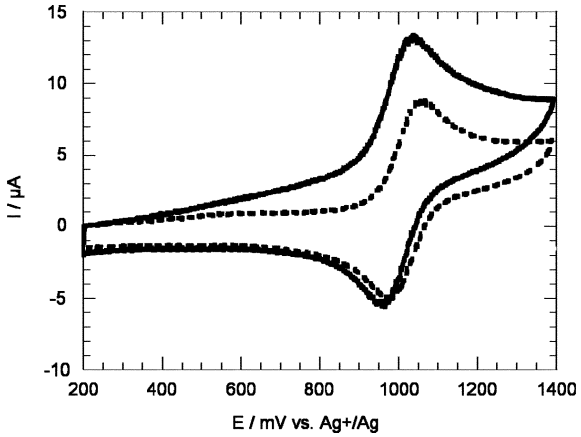

Fig. 6 Comparison of the CVs of the free ruthenium complex **2** (dotted line) and of Au-**2**-NCs (full line; $R = 2$; TEM image, see Fig. 2b) at 1 V s^{-1} in acetonitrile on a platinum electrode. Concentration of ruthenium: 1.5 mM.

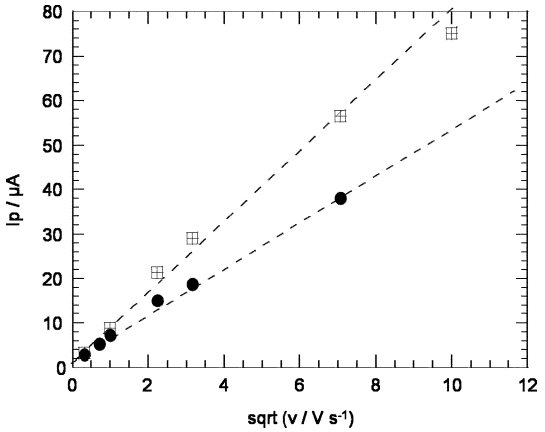

Fig. 7 Peak current *vs.* square root of the scan rate for the free ruthenium complex **2** (dots) and Au-**2**-NCs (squares).

contrary to what would be expected in case of electrostatic repulsions between adjacent redox moieties.[32] Actually the slightly negative potential shift for Au-**2**-NCs oxidation can not be explained on the basis of the donor effect of the modified phenanthroline ligand, like in similar ruthenium complexes in solution,[33] because the positive charge borne by the NP core should on the contrary favor the less charged redox state of the ruthenium. Conversely this potential shift could originate from the stabilization of the HOMO level of Ru(II) in Au-**2**-NCs compared to the free complex, in accordance with a kind of delocalized state involving all the ruthenium centres through the conductive NP.

Looking at the peak currents reveals that both free and grafted ruthenium complexes exhibit the same intensity values with a linear correlation of the peak current with the square root of scan rate in both cases (Fig. 7). This latter point is characteristic of a diffusion limited mass transfer. Nevertheless, in the case of functionalized colloids with nonredox active cores (like peripherally functionalized dendrimer systems),[30c] one would expect a much lower peak current for the grafted redox moiety *vs.* the free one, simply because of slower diffusion rates due to the larger size of the grafted system. This is not the case here, as confirmed by the comparison of the diffusion coefficient factor D, deduced from the slopes of the peak current *vs.* square root of scan rate curves.[34] It is likely that the difference observed between the grafted and free complexes is due to the ability of the former to accept a greater amount of charge, thus involving the storage capacity of the gold nanoparticle. It is well known that monolayer protected gold clusters are able to store charges through quantized double layer charging processes.[35] The capacitance is greater as the polarity and rigidity of the ligands constituting the protecting layer increases.[30b] Thus it is not surprising that in our case double layer charging of the gold core meaningfully contributes to the voltammetric current, as mentioned by Murray *et al.* in the case of viologen functionalized gold NP.[36] Thus our results show that conjugated linkers between the redox moiety and the metallic NP core enhances the ability of this latter for charge storage, leading to much higher currents than those forecast on the basis of classical diffusion models (Stokes–Einstein).

Table 4 Comparison of the electrochemical data between the free ruthenium complex **2** and Au-**2**-NCs in acetonitrile. E° is the standard potential determined from the average value of the anodic and the cathodic peak potentials. Values of D are deduced from the slopes of the peak current *vs.* square root of the scan rate (theoretical value for $Ru(phen)_3^{2+}$ in acetonitrile: $D = 1.65 \times 10^{-5}$ cm^2 s^{-1})

	C_{Ru}/mM	$D/10^{-5}$ cm^2 s^{-1}	E°/mV	ΔE_p/mV
Au-**2**-NCs	1.5	2.9	995	73
free ruthenium complex **2**	1.5	1.3	1020	73

Luminescence of Au-1-NCs in acetonitrile. Another interesting point to investigate is the influence of the NP on the emission properties of the grafted fluorophore. It has been shown that the metallic NP often quenches the fluorescence through charge or energy transfers,[37] but fluorescence enhancement can also be observed depending on various factors such as the distance between the metallic NP and the fluorophore or the nature of the fluorophore itself.[38,39] Therefore we

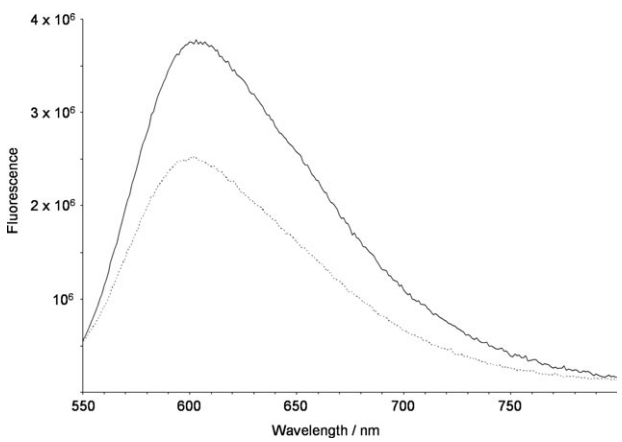

Fig. 8 Fluorescence spectra of the free ruthenium complex **1** (full line) and of Au-**1**-NCs (dotted line; $R = 2$; TEM image, see Fig. 2a) in acetonitrile under an argon atmosphere (*ca.* 5 µM in Ru).

recorded the emission spectra of the free ruthenium complex **1** and the Au-**1**-NCs in acetonitrile (Fig. 8). The concentration of each solution was adjusted in order to record the same absorbance at the excitation wavelength (453 nm) for both compounds, which corresponds to the MLCT band of the ruthenium complex **1**. The fluorescence spectra exhibit a maximum emission at 602 nm and clearly show a *ca*. 33% quenching for the grafted ruthenium complex *vs*. the free one. Quantum yields were calculated *vs*. a reference compound (4-(dicyanomethylene)-2-methyl-6-(*p*-dimethylaminostyryl)-4-*H*-pyran DCM in methanol)[22] and values of 3.5 and 2.3% were found for the free and grafted ruthenium complexes, respectively. In the present case, the emission maximum wavelength falls into the absorption band corresponding to the plasmon resonance, so that energy transfer is likely to be the major quenching process. Murray *et al*. have already reported such an energy transfer for $[Ru(bpy)_3]^{2+}$ electrostatically associated to Au-NP (1.3–3.9 nm in diameter).[37] Nevertheless, due to the rigid and fully conjugated character of the linker, electron transfer could also contribute to the deexcitation of the fluorophore. Time resolved fluorescence experiments are in progress to discriminate the role of these two processes. Moreover, the chemical nature of the link between the ruthenium complex and Au-NP and the Au-NP size dependence upon luminescence quenching are under investigation.

Conclusion

The control in different media of the stability, size and shape of nanoparticles, which are key factors for their specific chemical and physical properties, has always been a challenge and much attention has been paid to the comprehensive formation of nanocomposites. We demonstrated that polypyridyl ruthenium complexes bearing a phenanthroline, a pyridine or a thiophene terminal group could act as effective coating agents for the synthesis of gold or silver nanocomposites. We also showed that the solvent, nature of the metallic particles, ratio $R = [M^{n+}]/[Ru^{2+}]$ (M = Ag or Au) and amount of reducing agent are interdependent key parameters for the final stability, size and shape of the nanocomposites obtained. Several results must be pointed out:

• The amount of ruthenium complex and nature of the terminal group ensuring the interaction between the ruthenium complex and the metallic nanoparticle are crucial parameters for the stability, size and polydispersity of the final NCs. Indeed, a concomitant increase of $R = [M^{n+}]/[Ru^{2+}]$ (M = Ag or Au) and the size and polydispersity in size of the final NCs was usually detected. A weak interaction was usually observed with the monodentate thiophene group while a stronger interaction, leading to more monodisperse and stable colloidal solutions, was observed with the bidentate chelating phenanthroline group.

• Facetted NCs were only obtained with Au-NPs in water. In all other syntheses, nearly spherical NCs were observed.

• XPS proved to be a powerful technique for the characterization of the NCs. The remarkable reproducibility of the XPS measurements demonstrated that the metallic NPs are effectively coated by the ruthenium complexes but also showed that anions like Cl^- are full components of the NCs and play a crucial role for the stability of the NCs. A spontaneous exchange of these anions, leading to a purification of the NCs, can allow a reversible transfer in aqueous and non-aqueous solvents.

Preliminary electrochemical and luminescence measurements have shown the influence of the metallic NPs on the properties of the ruthenium complex. The ability to tune a vast range of characteristics of the ruthenium complex such as the nature of the pendant group ensuring the connection with the metallic particle, the length of the conjugated system and therefore the distance between the metallic particle and the ruthenium centre, will be used in order to understand and control the interaction between both components of the nanocomposites. Our NCs are unique in providing the opportunity to study the direct interaction of metallic NPs with metallic complexes through fully conjugated systems and further experiments are currently under way to elucidate the benefit of such connections in metallic nanocomposites.

References

1 See, for example: R. Bandyopadhyaya, W. Rong and S. K. Friedlander, *Chem. Mater*., 2004, **16**, 3147.
2 S. Reculusa, C. Mingotaud, E. Bourgeat-Lami, E. Duguet and S. Ravaine, *Nano Lett*., 2004, **4**, 1677.
3 S. D. Bunge, K. M. Krueger, T. J. Boyle, M. A. Rodriguez, T. J. Headley and V. L. Colvin, *J. Mater. Chem*., 2003, **13**, 1705.
4 See, for example: C. Louis, R. Bazzi, C. A. Marquette, J.-L. Bridot, S. Roux, G. Ledoux, B. Mercier, L. Blum, P. Perriat and O. Tillement, *Chem. Mater*., 2005, **17**, 1673.
5 See, for example: M. C. Daniel and D. Astruc, *Chem. Rev*., 2004, **104**, 293.
6 R. Méallet-Renault, R. Pansu, S. Amigoni-Gerbier and C. Larpent, *Chem. Commun*., 2004, 2344.
7 E. Beaurepaire, V. Buissette, M.-P. Sauviat, D. Giaume, K. Lahlil, A. Mercuri, D. Casanova, A. Huignard, J.-L. Martin, T. Gacoin, J.-P. Boilot and A. Alexandrou, *Nano Lett*., 2004, **4**, 2079.
8 P. Hazarika, B. Ceyhan and C. M. Niemeyer, *Angew. Chem., Int. Ed*., 2004, **43**, 6469.
9 Y.-S. Shon and H. Choo, *Chem. Commun*., 2002, 2560.
10 M.-C. Daniel, J. Ruiz, S. Nlate, J.-C. Blais and D. Astruc, *J. Am. Chem. Soc*., 2003, **125**, 2617.
11 M. Brust, M. Walker, D. Bethell, D. J. Schiffrin and R. J. Whyman, *J. Chem. Soc., Chem. Commun*., 1994, 801.
12 W. Wang, X. Chen and S. Efrima, *J. Phys. Chem. B*, 1999, **103**, 7238.
13 A. Moores, F. Goettmann, C. Sanchez and P. Le Floch, *Chem. Commun*., 2004, 2842.
14 L. M. Liz-Marzán, M. Giersig and P. Mulvaney, *Langmuir*, 1996, **12**, 4329.
15 C. R. Mayer, S. Neveu and V. Cabuil, *Angew. Chem., Int. Ed*., 2002, **41**, 501.
16 C. R. Mayer, S. Neveu, C. Simonnet-Jégat, C. Debiemme-Chouvy, V. Cabuil and F. Sécheresse, *J. Mater. Chem*., 2003, **13**, 338.
17 C. R. Mayer, E. Dumas and F. Sécheresse, *Chem. Commun*., 2005, 345.
18 (*a*) J. Kim, J. E. Lee, J. Lee, Y. Jang, S. -W. Kim, K. An, J. H. Yu and T. Hyeon, *Angew. Chem., Int. Ed*., 2006, **45**, 4789; (*b*) V. J. Gandubert and R. B. Lennox, *Langmuir*, 2006, **22**, 4589; (*c*) J. Cho and F. Caruso, *Chem. Mater*., 2005, **17**, 4547.
19 E. Amouyal, A. Homsi, J.-C. Chambron and J.-P. Sauvage, *J. Chem. Soc., Dalton Trans*., 1990, 1841.
20 C. Hiort, P. Lincoln and B. Nordén, *J. Am. Chem. Soc*., 1993, **115**, 3448.
21 D. Garreau and J. M. Savéant, *J. Electroanal. Chem*., 1975, **50**, 1.
22 J. M. Drake, M. L. Lesiecki and D. M. Camaioni, *Chem. Phys. Lett*., 1985, **113**, 530.

23 S. R. Isaacs, E. C. Cutler, J. -S. Park, T. Randall Lee and Y. -S. Shon, *Langmuir*, 2005, **21**, 5689.
24 D. Astruc, F. Lu and J. R. Aranzaes, *Angew. Chem., Int. Ed.*, 2005, **44**, 7852.
25 X. Liu, K. G. Neoh and E. T. Kang, *Langmuir*, 2002, **18**, 9041.
26 J. Fink, C. J. Kiely, D. Bethell and D. J. Schiffrin, *Chem. Mater.*, 1998, **10**, 922.
27 R. E Shepherd, A. Proctor, W. W. Henderson and T. K. Myser, *Inorg. Chem.*, 1987, **26**, 2440.
28 H. Gong and M. Liu, *Langmuir*, 2001, **17**, 6228.
29 R. M. Leasure, W. Ou, J. A. Moss, R. W. Linton and T. J. Meyer, *Chem. Mater.*, 1996, **8**, 264.
30 (*a*) M. J. Hostetler, S. J. Green, J. J. Stokes and R. W. Murray, *J. Am. Chem. Soc.*, 1996, **118**, 4212; (*b*) S. Chen and K. Huang, *Langmuir*, 2000, **16**, 2014; (*c*) A. Laborde, J. Ruiz and D. Astruc, *J. Am. Chem. Soc.*, 2002, **124**, 1782.
31 A. J. Bard and L. R. Faulkner, *Electrochemical Methods*, Wiley, New York, 2nd edn, 2000, ch. 12.
32 W. S. Baker, B. I. Lemon III and R. M. Crooks, *J. Phys. Chem. B*, 2001, **105**, 8885.
33 B. H. Kim, D. N. Lee, H. J. Park, J. H. Min, Y. M. Jun, S. J. Park and W.-Y. Lee, *Talanta*, 2004, **62**, 595.
34 The influence of the electroactive area of the electrode (instead of the geometric area) is taken into account by using a ferrocene probe in the same conditions.
35 J. F. Hicks, D. T. Miles and R. W. Murray, *J. Am. Chem. Soc.*, 2002, **124**, 13322.
36 A. C. Templeton, D. E. Cliffel and R. W. Murray, *J. Am. Chem. Soc.*, 1999, **121**, 7081.
37 P. P. H. Cheng, D. Silvester, G. Wang, G. Kalyuzhny, A. Douglas and R. W. Murray, *J. Phys. Chem. B*, 2006, **110**, 4637, and references therein.
38 O. G. Tovmachenko, C. Graf, D. J. van den Heuvel, A. van Blaaderen and H. C. Gerritsen, *Adv. Mater.*, 2006, **18**, 91.
39 K. G. Thomas and P. V. Kamat, *J. Am. Chem. Soc.*, 2000, **122**, 2655.